ELSEVIER

Chemico-Biological Interactions 128 (2000) 65–90

Chemico-Biological Interactions

www.elsevier.com/locate/chembiont

Synthesis and structure determination of 6-methylbenzo[*a*]pyrene-deoxyribonucleoside adducts and their identification and quantitation in vitro and in mouse skin

Aaron A. Hanson [a], Kai-Ming Li [a], Cheng-Huang Lin [b], Ryszard Jankowiak [c], Gerald J. Small [b,c], Eleanor G. Rogan [a], Ercole L. Cavalieri [a,*]

[a] *Eppley Institute for Research in Cancer and Department of Pharmaceutical Sciences, University of Nebraska Medical Center, Omaha, NE 68198-6805, USA*

[b] *Department of Chemistry, Iowa State University, Ames, IA 50011, USA*

[c] *Ames Laboratory-USDOE, Iowa State University, Ames, IA 50011, USA*

Accepted 21 June 2000

Abstract

Activation of the moderate carcinogen 6-methylbenzo[*a*]pyrene (6-CH_3BP) by one-electron oxidation to form DNA adducts was studied. Iodine oxidation of 6-CH_3BP in the presence of dGuo produces BP-6-CH_2-N^2dGuo, BP-6-CH_2-N7Gua and a mixture of 6-CH_3BP-(1&3)-N7Gua, whereas in the presence of Ade the adducts BP-6-CH_2-N1Ade, BP-6-CH_2-N3Ade, BP-6-CH_2-N7Ade and 6-CH_3BP-(1&3)-N1Ade are obtained. Furthermore, for the first time an aromatic hydrocarbon radical cation afforded an adduct with dThd, the stable adduct

Abbreviations: BP, benzo[*a*]pyrene; BP-6-CH_2-N3Ade, 3-(benzo[a]pyren-6-methylenyl)adenine; BP-6-CH_2-N7Ade, 7-(benzo[*a*]pyren-6-methylenyl)adenine; BP-6-CH_2-N7Gua, 7-(benzo[*a*]pyren-6-methylenyl)guanine; 6-CH_3BP, 6-methylbenzo[*a*]pyrene; 6-CH_3BP-(1&3)-N7Gua, 7-(6-Methylbenzo[*a*]pyren-1&3-yl)guanine; COSY, 2-dimensional chemical shift correlation spectroscopy; DMF, dimethylformamide; DMSO, dimethylsulfoxide; FAB MS/MS, fast atom bombardment tandem mass spectrometry; FLNS, fluorescence line narrowing spectroscopy; HRP, horseradish peroxidase; MC, 3-methylcholanthrene; NLN, non-line narrowed; NOE, nuclear Overhauser effect; PAH, polycyclic aromatic hydrocarbon(s); PDA, photodiode array.

* Corresponding author. Tel.: +1-402-5597237; fax: +1-402-5598068.

E-mail address: ecavalie@mail.unmc.edu (E.L. Cavalieri).

PII: S0009-2797(00)00189-7

BP-6-CH_2-N3dThd. Formation of these adducts indicates that the 6-CH_3BP radical cation has charge localized at the 6, 1 and 3 position. When 6-CH_3BP was activated by horseradish peroxidase in the presence of DNA, two depurinating adducts were identified, BP-6-CH_2-N7Gua (48%) and 6-CH_3BP-(1&3)-N7Gua (23%), with 29% unidentified stable adducts. In the binding of 6-CH_3BP catalyzed by rat liver microsomes, the same two depurinating adducts, BP-6-CH_2-N7Gua (22%) and 6-CH_3BP-(1&3)-N7Gua (10%), were identified, with 68% unidentified stable adducts. In 6-CH_3BP-treated mouse skin, the two depurinating adducts, BP-6-CH_2-N7Gua and 6-CH_3BP-(1&3)-N7Gua, were identified. Although quantitation of these two adducts was not possible due to coelution of metabolites on HPLC, they appeared to be the major adducts found in mouse skin. These results show that 6-CH_3BP forms depurinating adducts only with the guanine base of DNA, both in vitro and in mouse skin. The weaker reactivity of 6-CH_3BP radical cation vs. BP radical cation could account for the weaker tumor-initiating activity of 6-CH_3BP in comparison to that of BP.

Keywords: 6-Methylbenzo[*a*]pyrene-deoxyribonucleoside adducts; Mouse skin; Carcinogen

1. Introduction

Polycyclic aromatic hydrocarbons (PAH) undergo two main pathways of metabolic activation related to tumor initiation: one-electron oxidation to give radical cations and monooxygenation with formation of bay-region diol epoxides [1–3]. Activation of PAH can proceed through either of these pathways, or both, to form stable and depurinating DNA adducts. The stable adducts remain covalently bound to DNA, whereas depurinating adducts are eliminated from DNA by cleavage of the glycosyl bond. Determination of the structure of DNA adducts provides information on the mechanism of activation, the type of DNA damage, and the biological significance in terms of tumor initiation. A relationship has been established between Harvey-*ras* mutations in mouse skin papillomas and apurinic sites generated by loss of depurinating PAH-DNA adducts [4].

To elucidate mechanisms of tumor initiation, the profile of DNA adducts formed by benzo[*a*]pyrene (BP) in vitro and in vivo has been determined [5,6]. In mouse skin, 71% of the total adducts are depurinating adducts. Of these, 66% are formed from BP radical cation, with specific reaction at C-6 [6]. Some DNA adducts of 6-fluoroBP and 6-methylbenzo[*a*]pyrene (6- CH_3BP) have been synthesized by electrochemical oxidation [7], and the stable adducts formed by these two PAH in vitro have been investigated [8]. Tumorigenicity studies of BP, 6-fluoroBP, 6-CH_3BP, 6-chloroBP, and 6-bromoBP show that 6-fluoroBP and 6-CH_3BP are active [9,11], but less potent than the parent compound, whereas 6-chloroBP and 6-bromoBP are virtually inactive [9,10].

6-CH_3BP contains a methyl substituent at the critical C-6, the preferred position in which the BP radical cation binds to nucleophiles. Charge localization of the 6-CH_3BP radical cation at C-6 renders the methyl group reactive with nucleophiles. This has been observed in the oxidation of 6-CH_3BP by manganic acetate, as well as in electrochemical oxidation of 6-CH_3BP in the presence of dGuo [7,12]. In these

reactions, nucleophilic attack at the methyl group of the 6-CH_3BP radical cation competes with attack at the positions of second highest reactivity, C-1 and C-3. This suggests that the reactivity of the methyl group in 6-CH_3BP radical cation is less than that of C-6 in BP radical cation, in which no adducts are obtained at C-1 or C-3 [12–15].

In this paper, we report the synthesis of standard DNA adducts substituted at the 6-methyl group, and at C-1 and C-3, obtained by iodine oxidation of 6-CH_3BP in the presence of deoxyribonucleosides and nucleobases. This method yields adducts that are not obtained by electrochemical oxidation [7]. We also report the identification of biologically formed 6-CH_3BP-DNA depurinating adducts by comparison with the synthesized standard adducts. Total stable adducts were quantitated by the ^{32}P-postlabeling method [16]. Knowledge of the DNA adducts formed by 6-CH_3BP is necessary for understanding the biological significance of the adducts in producing the mutations leading to cancer.

2. Methods and materials

Caution. The chemicals 6-CH_3BP and BP are hazardous and should be handled carefully in accordance with NIH guidelines [17].

2.1. Chemicals

6-CH_3BP was synthesized as described below. 6-CH_3BP-7,8-dihydrodiol was prepared enzymatically, isolated by preparative HPLC, and identified by its characteristic UV spectrum, similar to that of BP-7,8-dihydrodiol and its retention time on HPLC, that corresponds to the most polar metabolite after the 4,5-dihydrodiol [8]. The high polarity of 6-CH_3BP-7,8-dihydrodiol is due to the diaxial conformation of the two hydroxy groups. The dGuo, dAdo and dThd (TCI, Portland, OR) were desiccated over P_2O_5 under vacuum at 110°C for 48 h prior to use. Ade and Gua (P-L Biochemicals,), BP, I_2, anhydrous dimethylformamide (DMF) and dimethylsulfoxide (DMSO) (Aldrich, Milwaukee, WI), HPLC-grade organic solvents (EM Science, Gibbstown, NJ), $AgClO_4$ (GFS Chemicals, Columbus, OH), and $Na_2S_2O_3$ (Fisher Scientific, Fair Lawn, NJ) were used as obtained.

2.2. HPLC

Analytical HPLC was conducted on a Waters 600E solvent delivery system equipped with a Waters 700 WISP autoinjector. Effluents were monitored for UV absorbance (254 nm) with a Waters 996 photodiode array (PDA) detector. Biological samples were also monitored for fluorescence with a Waters 474 scanning fluorescence detector. Runs were conducted on a YMC (YMC, Overland Park, KS) ODS-AQ 5-μm 120-Å column (4.6 × 250 mm or 6 × 250 mm, analytical) at a flow rate of 1 mL/min. Preparative HPLC was conducted on a Waters 600E solvent delivery system coupled with a Waters 990 PDA. Runs were conducted on a YMC

ODS-AQ 5-μm 120-Å column (20 × 250 mm) at a flow rate of 8 ml/min. UV absorbance was recorded during HPLC separations with a Waters 990 PDA detector.

2.3. NMR

Proton, homonuclear two-dimensional chemical shift correlation spectroscopy (COSY) and nuclear Overhauser effect (NOE) NMR spectra were recorded on a Varian Unity 500 at 499.835 MHz in DMSO-d_6 at 26°C.

2.4. Mass spectrometry

Fast atom bombardment tandem mass spectrometry (FAB MS/MS) was performed at the Nebraska Center for Mass Spectrometry using a Micromass (Manchester, England) AutoSpec high resolution magnetic sector mass spectrometer. The instrument was equipped with an orthogonal acceleration time-of-flight serving as the second mass spectrometer in the tandem experiment. Xenon was admitted to the collision cell at a level to attenuate the precursor ion signal by 75%. Data acquisition and processing were accomplished using OPUS software that was provided by the manufacturer (Microcasm). Samples were dissolved in 5–10 μl of CH_3OH; 1-μl aliquots were placed on the sample probe tip along with 1 μl of a 1:1 mixture of glycerol/thioglycerol.

2.5. Fluorescence line narrowing spectroscopy (FLNS)

The details of the instrumentation used for low temperature laser-excited FLNS have been reported elsewhere [18]. Briefly, FLN spectra ($S_1 \leftarrow S_0$ excitation) at $T = 4.2$ K were obtained by a Lambda Physik-FL2002 dye laser pumped by a Lambda Physik Lextra XeCl excimer laser as the excitation source. Several excitation wavelengths were used, each revealing a portion of the S_1 excited-state vibrational frequencies of 6-CH_3BP-derived DNA adducts. Samples were dissolved in C_2H_5OH (see below) and cooled with liquid helium in a glass cryostat with quartz optical windows. Fluorescence was dispersed by a McPherson 2061 1-meter focal length monochromator and detected by a Princeton Instruments IRY 1024/GRB intensified PDA. For time-resolved detection, a Princeton Instruments FG-100 pulse generator was employed; the gate width was set to 200 ns and various delay times (0–100 ns) were used. Spectral resolution used for FLN measurements was 0.05 nm.

2.6. Synthesis of 6-CH_3BP

BP (1 g, 3.96 mmol) was dissolved in 30 ml of anhydrous CH_2Cl_2 under a nitrogen atmosphere in a 100-ml round bottom flask and placed in an ice bath. After 15 min, 1,1-dichloromethylether (11.88 mmol) and anhydrous Tin(IV)chloride (13.9 mmol) in CH_2Cl_2 were added. The reaction mixture was stirred for 20 h and

was analyzed by TLC using hexane as the elutant. The reaction mixture contained the less polar starting material, BP, and 6-formylBP. An additional 3 eq of 1,1-dichloromethylether and 3.5 eq of Tin(IV)chloride were added, and the mixture was allowed to react for another 20 h.

$CHCl_3$ (100 ml) and brine (100 ml) were added to the reaction mixture. The $CHCl_3$ layer was separated and the brine solution extracted twice with $CHCl_3$ (100 ml). The $CHCl_3$ extracts were evaporated to dryness and the resulting solid was chromatographed on a silica column (2.5×30 cm) in 100% hexane. Hexane was used to elute the unreacted BP and 20–50% $CHCl_3$ in hexane was used to elute 6-formylBP. 6-FormylBP was then converted to 6-CH_3BP by the method of Dewhurst and Kitchen [19]. Yields from starting material, BP, to products were 69% for 6-formylBP and 59% for 6-CH_3BP.

2.7. Synthesis of 6-CH_3BP adducts by iodine oxidation

Glassware, syringes and needles were dried at 150°C prior to use. The reaction glassware was assembled while hot, cooled under vacuum and pressurized under an inert atmosphere (argon or nitrogen). Syringes and needles were cooled under vacuum in a desiccator and pressurized under an inert atmosphere. All reaction flasks were silated with Silanization Solution I (Fluka, Ronkonkoma, NY). Coupling between 6-CH_3BP and the nucleophiles was accomplished by combining 15 mg (56 μmol) of 6-CH_3BP with 5 eq of dGuo, dAdo, Ade or Gua dissolved in 3.5 mL of DMSO or DMF in a 50-ml three-necked flask, as previously described in detail [15].

2.8. Synthesis of BP-6-CH_2-N3dThd by electrochemical oxidation

Electrochemical synthesis was conducted with a previously described apparatus (EG&G Princeton Applied Research, Princeton, NJ) [13]. The oxidation potential for 6-CH_3BP is 0.95 V in DMF, whereas dThd has an anodic peak potential > 1.40 V. Therefore, during adduct synthesis dThd was not oxidized.

Glassware, syringe, needles, electrochemical cell and platinum working and reference electrodes were dried at 150°C prior to use. the electrochemical cell and electrodes were assembled while hot and then cooled under argon.

DMF (35 ml) containing 0.5 M $KClO_4$ as the supporting electrolyte was pre-electrolyzed at 1.45 V, while argon was bubbled in the cell, until no appreciable current could be detected (ca. 30 min). The dThd (85 mg, 376 μmol) and 6-CH_3BP (10 mg, 37.6 μmol) were added as solid; when the solid dissolved, the cell was switched on, and the electrode potential was gradually increased from 0 to 0.95 V, and kept constant at this value during the entire electrolysis. The reaction was stopped when the output current (I) had decreased to ca. 5% of the initial value and a charge 2.0 times the theoretical charge expected for two-electron transfer had accumulated, ca. 3 h.

After reaction was complete, the DMF was evaporated under vacuum, and the adduct was extracted four times from the solid residue by using a solvent mixture

of $C_2H_5OH/CHCl_3/CH_3COCH_3$ (2:1:1), and the resulting extract was filtered through a Whatman fluted filter paper. The combined solvent mixture was evaporated under vacuum; the residue was dissolved in 3 mL of DMSO, and the crude adduct was analyzed by HPLC with the CH_3CN/H_2O analytical gradient (Table 1). Purification of the adduct was conducted with preparative HPLC with the CH_3CN/H_2O gradient (Table 1), followed by a CH_3OH/H_2O gradient. The yield (8%) of the adduct was determined by monitoring absorbance at 254 nm during HPLC separation.

2.9. Analysis of adduct structures

For HPLC analysis, the reaction mixture was dried under vacuum at 50°C, redissolved in 4 ml $DMSO/C_2H_5OH$ (1:1), and filtered through a 0.45-μm filter. The filter was then washed with an additional 500 μl of DMSO. Determination of the yield of the synthesized adducts was accomplished by analytical or semipreparative HPLC, in either CH_3CN/H_2O, CH_3OH/H_2O or $C_2H_5OH/CH_3CN/H_2O$ solvent systems (Table 1), with monitoring at 254 nm for comparison of peak areas of adduct(s), by-product(s), and parent compound (Table 2). The percentage of each adduct in Table 2 was calculated by dividing the peak area of the adduct by the sum of the peak areas of the adduct(s), by-product(s), and parent compound.

Table 1
Analytical, semipreparative, and preparative HPLC gradients for the separation of adducts[a]

6-CH_3BP-dGuo or Gua, analytical and preparative		6-CH_3BP-dAdo or Ade, analytical and preparative	
Time[b]	CH_3OH	Time	C_2H_5OH/CH_3CN[d]
0–15	50%[c]	0–15	30%
25–35	75%	30–40	70%
45	100%	50	100%
6-CH_3BP-Ade, preparative (second purification)		6-CH_3BP biological adducts, analytical (first purification)	
Time	CH_3CN	Time	CH_3CN
0–5	30%	0–5	20%
60	100%	85	100%
6-CH_3BP-(1&3)-N7Gua, analytical (second purification)		BP-6-CH_2-N7Gua, analytical (second purification)	
Time	CH_3OH	Time	C_2H_5OH/CH_3CN[d]
0–5	30%	0–15	30%
70	100%	30–40	70%
		50	100%

[a] All gradients were linear, except for 6-CH_3BP-(1&3)-N7Gua, analytical (second purification), which used a convex (CV5) gradient.

[b] Time is in min.

[c] The organic phase starts as a mixture with water.

[d] The C_2H_5OH/CH_3CN organic phase is a 3:1 mixture, respectively.

Table 2
Yield of adducts formed when 6-CH_3BP was reacted with dGuo, Gua, dAdo or Ade in the presence of I_2 in DMF or DMSO[a]

Nucleoside/base	Adducts	% Adduct formed	
		DMF	DMSO
dGuo	BP-6-CH_2-N7Gua	14	14
	6-CH_3BP-(1&3)-N7Gua	4	2
	BP-6-CH_2-N^2dGuo	13	27
Gua	BP-6-CH_2-N7Gua		13
	6-CH_3BP-(1&3)-N7Gua		13
	BP-6-CH_2-N^2Gua		9
dAdo	BP-6-CH_2-N7Ade	35	28
Ade	BP-6-CH_2-N1Ade	75	70
	6-CH_3BP-(1&3)-N1Ade	75	70
	BP-6-CH_2-N7Ade (Minor)	75	70
	BP-6-CH_2-N3Ade (Minor)	75	70

[a] The percentage of adduct is relative to the amount of starting 6-CH_3BP. The remainder is starting material. Each reaction was carried out at least three times.

Purification of the adducts was conducted by preparative or semipreparative HPLC, as listed in Table 1. Reactions conducted with Ade were analyzed in a $C_2H_5OH/CH_3CN/H_2O$ solvent system due to the insolubility of the 6-CH_3BP-N1Ade adducts in either CH_3CN/H_2O or CH_3OH/H_2O solvent systems.

Known adducts were identified by comparing analytical HPLC retention time, UV spectra and 500 MHz ^{1}H NMR (DMSO, 2.49 ppm at 26°C) to those previously obtained [6]. Novel adducts were identified by a combination of UV spectra, 500 MHz ^{1}H NMR, including NOE, D_2O exchange and COSY, and FAB MS/MS.

2.9.1. 7-(Benzo[a]pyren-6-methylenyl)Gua (BP-6-CH_2-N7Gua)

UV λ_{max} (nm) 267, 291, 303, 360, 378, 398; ^{1}H NMR, δ (ppm): 6.25 (s, 2H, 6-CH_2), 6.79 (bs, 2H, 2-NH_2[Gua]), 6.99 (s, 1H, 8-H[Gua]), 7.90 (m, 2H, 8-H, 9-H), 8.10 (dd, 1H, $J_{1,2} = 7.5$ Hz, $J_{2,3} = 7.5$ Hz, 2-H), 8.20 (d, 1H, $J_{4,5} = 9.5$ Hz, 4-H), 8.28 (d, 1H, $J_{2,3} = 7.5$ Hz, 3-H), 8.43 (d, 1H, $J_{1,2} = 7.5$ Hz, 1-H), 8.52 (d, 1H, $J_{11,12} = 9.5$ Hz, 12-H), 8.67 (d, 1H, $J_{4,5} = 9.5$ Hz, 5-H), 8.70 (d, 1H, $J_{7,8} = 8.0$ Hz, 7-H), 9.34 (m, 2H, 10-H, 11-H); FAB MS: $(M + H)^+$ $C_{26}H_{18}N_5O$:438.1316 (calcd 438.1331).

2.9.2. N^2-(Benzo[a]pyren-6-methylenyl)dGuo (BP-6-CH_2-N^2dG)

UV λ_{max} (nm) 267, 290, 302, 358, 376, 396; ^{1}H NMR, δ (ppm): 2.36 (m,1H, 2′-H), 2.74 (m, 1H, 2′-H), 3.60 (m, 1H, 5′-H), 3.63 (m, 1H, 5′-H), 3.92 (s, 1H, 4′-H), 4.47 (s, 1H, 3′-H), 4.99 (bs, 1H, 5′-OH), 5.44 (s, 1H, 3′-OH), 5.62 (s, 2H, 6-CH_2), 6.44 (t, $J_{1',2'} = 7.0$ Hz, 1H, 1′-H), 7.92 (bs, 1H, 2-NH[Gua]), 7.93 (m, 2H, 8-H, 9-H), 7.99 (s, 1H, 8-H[Gua]), 8.07 (dd, 1H, $J_{1,2} = 7.5$ Hz, $J_{2,3} = 7.5$ Hz, 2-H), 8.18 (d, 1H,

$J_{4,5}$ = 9.5 Hz, 4-H), 8.24 (d, 1H, $J_{2,3}$ = 7.5 Hz, 3-H), 8.38 (d, 1H, $J_{1,2}$ = 7.5 Hz, 1-H), 8.47 (d, 1H, $J_{11,12}$ = 9.5 Hz, 12-H), 8.63 (d, 1H, $J_{4,5}$ = 9.5 Hz, 5-H), 8.76 (m, 1H, 7-H), 9.30 (d, 1H, $J_{11,12}$ = 9.5 Hz, 11-H), 9.32 (d, 1H, $J_{9,10}$ = 8.0 Hz, 10-H); FAB MS: $(M+H)^+$ $C_{26}H_{18}N_5O$:532.1988 (calcd 532.1985).

2.9.3. 1-(Benzo[a]pyren-6-methylenyl)Ade (BP-6-CH_2-N1Ade)

UV λ_{max} (nm) 267, 294, 301, 357, 377, 396; ^{1}H NMR, δ (ppm) 6.72 (s, 2H, 6-CH_2), 7.64 (s, 1H, 2-H[Ade]), 7.83 (dd, 2H, $J_{7,8}$ = 7.0 Hz, $J_{8,9}$ = 7.0 Hz, 8-H, 6-NH[Ade]), 7.91 (dd, 2H, $J_{8,9}$ = 7.0 Hz, $J_{9,10}$ = 7.0 Hz, 9-H, 6-NH[Ade]), 7.98 (s, 1H, 8-H[Ade]), 8.11 (dd, 1H, $J_{1,2}$ = 7.5 Hz, $J_{2,3}$ = 7.5 Hz, 2-H), 8.20 (d, 1H, $J_{4,5}$ = 10.0 Hz, 4-H), 8.29 (d, 1H, $J_{2,3}$ = 7.5 Hz, 3-H), 8.44 (d, 1H, $J_{1,2}$ = 7.5 Hz, 1-H), 8.45 (d, 1H, $J_{11,12}$ = 9.5 Hz, 12-H), 8.67 (m, 2H, 5-H, 7-H), 9.34 (m, 2H, 10-H, 11-H); FAB MS: $(M+H)^+$ $C_{26}H_{18}N_5O$:400.1545 (calcd 400.1562).

2.9.4. 1-(6-methylbenzo[a]pyren-1 & 3-yl)Ade [6-CH_3BP-(1&3)-N1Ade]

UV λ_{max} (nm) 268, 295, 305, 386, 404; ^{1}H NMR, δ (ppm): 3.22 (s, 3H, 6-CH_3), 7.36 (d, 1H, $J_{1,2}$ = 9.5 Hz, 4-H[3]), 7.66 (m, 2H, 12-H[1], 8-H[Ade]), 7.94 (m, 4H, 8-H[1,3], 9-H[1,3]), 8.21 (m, 2H, 4-H[1], 2-H[3]), 8.25 (d, $J_{2,3}$ = 7.5 Hz, 2H, 2-H[1], 6-NH[Ade]), 8.33 (bs, 1H, 6-NH[Ade]), 8.38 (d, $J_{2,3}$ = 7.5 Hz, 1H, 3-H[1]), 8.51 (m, 3H, 1-H[3], 5-H[3], 12-H[3]), 8.66 (m, 4H, 5-H[1], 7-H[1,3], 2-H[Ade]), 9.22 (m, 1H, 10-H[1]), 9.23 (d, 1H, $J_{11,12}$ = 9.5 Hz, 11-H[1]), 9.35 (m, 1H, 10-H[3]), 9.41 (d, 1H, $J_{11,12}$ = 9.5 Hz, 11-H[3]); FAB MS: $(M+H)^+$ $C_{26}H_{18}N_5O$:400.1555 (calcd 400.1562).

2.9.5. 3-(Benzo[a]pyren-6-methylenyl)Ade (BP-6-CH_2-N3Ade)

UV λ_{max} (nm) 266, 290, 302, 358, 376, 396; ^{1}H NMR, δ (ppm): 6.49 (s, 2H, 6-CH_2), 7.28 (bs, 2H, 6-NH_2[Ade]), 7.56 (s, 1H, 2-H[Ade]), 7.88 (m, 2H, 8-H, 9-H), 8.10 (m, 1H, 2-H), 8.24 (d, 1H, $J_{4,5}$ = 9.5 Hz, 4-H), 8.28 (d, 1H, $J_{2,3}$ = 7.5 Hz, 3-H), 8.35 (s, 1H, 8-H[Ade]), 8.43 (d, 1H, $J_{1,2}$ = 7.5 Hz, 1-H), 8.53 (d, 1H, $J_{11,12}$ = 9.5 Hz, 12-H), 8.74 (m, 2H, 5-H, 7-H), 9.33 (m, 2H, 10-H, 11-H); FAB MS: $(M+H)^+$ $C_{26}H_{18}N_5O$:400.1544 (calcd 400.1562).

2.9.6. 7-(Benzo[a]pyren-6-methylenyl)Ade (BP-6-CH_2-N7Ade)

UV λ_{max} (nm) 266, 290, 302, 360, 377, 397; ^{1}H NMR, δ (ppm): 6.72 (s, 2H, 6-CH_2), 7.10 (s, 1H, 8-H[Ade]), 7.38 (bs, 2H, 6- NH_2[Ade]), 7.87 (m, 1H, 8-H), 7.93 (m, 1H, 9-H), 8.11 (m, 1H, 2-H), 8.18 (d, 1H, $J_{4,5}$ = 9.5 Hz, 4-H), 8.26 (s, 1H, 2-H[Ade]), 8.29 (d, 1H, $J_{2,3}$ = 7.5 Hz, 3-H), 8.46 (m, 3H, 1-H, 5-H, 7-H), 8.57 (d, 1H, $J_{11,12}$ = 9.5 Hz, 12-H), 9.38 (m, 2H, 10-H, 11-H); FAB MS: $(M+H)^+$ $C_{26}H_{18}N_5O$:400.1561 (calcd 400.1562).

2.9.7. 3-(Benzo[a]pyren-6-methylenyl)dThd (BP-6-CH_2-N3dThd)

UV, λ_{max}(nm) 268, 288, 300, 312; ^{1}H NMR, δ (ppm) 0.85 (s, 3H, 5-CH_3[Thy]), 1.95-1.98 (m, 2H, 2′-H_2), 3.92-3.97 (m, 2H, 5′-H_2), 4.05 (m, 1H, 4′-H), 4.30 (m, 1H, 3′-H), 5.30 (s, 1H, 5′-OH, exchangeable with D_2O), 5.59 (s, 1H, 3′-OH, exchangeable with D_2O), 5.64-5.71 (m, 2H, 6-CH_2), 6.14 (t, 1H,1′H), 7.28 (s, 1H, 6-H[Thy]),

7.73-7.91 (m, 2H, 8-H,9-H), 8.04-8.10 (m, 1H, 2-H), 8.14 (d, 1H, 4-H, $J_{4,5} = 9.5$ Hz), 8.24 (d, 1H, 3-H, $J_{2,3} = 7.0$ Hz), 8.43 (d, 1H, 1-H, $J_{1,2} = 8.5$ Hz), 8.46-8.48 (d, 1H, 12-H, $J_{11,12} = 9.5$ Hz), 8.54 (d, 1H, 5H, $J_{4,5} = 9.5$ Hz), 8.73 (m, 1H, 7-H), 9.24-9.29 (m, 2H, 10-H, 11-H) FAB MS: $(M + H)^+$ $C_{31}H_{27}N_2O_5$:507.1911 (calcd 507.1920).

2.10. Binding of 6-CH_3BP to DNA in vitro

6-CH_3BP (80 μM) was bound to calf thymus DNA (1mg/mL, Pharmacia, Piscataway, NJ) in reactions catalyzed by 3-methylcholanthrene (MC)-induced rat liver microsomes (1 mg protein/mL) as previously described [20] or horseradish peroxidase (HRP, Sigma, St. Louis) as previously described [13]. All reactions were 15 mL in volume; they were incubated for 1 h at 37°C. For reactions with single-stranded DNA, calf thymus DNA was denatured by heating in a boiling water bath for 10 min, followed by quick cooling in an ice bath.

At the end of the reactions, a 1-ml aliquot of the mixture was used to determine the amount of stable DNA adducts by the P_1-nuclease-modified ^{32}P-postlabeling method, as previously described [16]. The DNA from the remaining 14-ml mixture was precipitated with two volumes of C_2H_5OH, and the supernatant was used to identify and quantify the depurinating adducts by HPLC and FLNS.

2.11. Binding of 6-CH_3BP to DNA in mouse skin

Two groups of nine female Swiss mice (8 weeks old, Eppley Colony) were treated on an area of shaved dorsal skin with 200 nmol of 6-CH_3BP in 50 μl of acetone. The mice were killed after 4 h, and the treated area was excised. Epidermis from each group was prepared, pooled, ground in liquid N_2 and 500 mg was taken to purify the DNA and to analyze the stable adducts by the ^{32}P-postlabeling method. The remainder was Soxhlet-extracted for 72 h with $CHCl_3/CH_3OH$ (1:1) or $CHCl_3/C_2H_5OH$ (1:1) to recover the depurinating adducts, and the adducts were analyzed by HPLC and FLNS.

2.12. Binding of 6-CH_3BP and 6-CH_3BP-7,8-dihydrodiol to DNA in mouse skin

6-CH_3BP was metabolized to the diaxial 6-CH_3BP-7,8-dihydrodiol by MC-induced rat liver microsomes at only a 0.1% yield. This metabolite was identified by a combination of its UV absorption spectrum and its retention time on HPLC, in which it is the second most polar metabolite after the 4,5-dihydrodiol. The same microsomes metabolized BP to its 7,8-dihydrodiol in a 1% yield, tenfold higher compared to 6-CH_3BP. Because the yield of the 6-CH_3BP-7,8-dihydrodiol was so low, only 72.2 nmol was isolated to treat mouse skin and analyze the stable DNA adducts formed.

One female Swiss mouse (8 weeks old, Eppley Colony) was treated on an area of shaved dorsal skin with 200 nmol of 6-CH_3BP in 50 μl of acetone. Another female Swiss mouse (8 weeks old, Eppley Colony) was treated on an area of shaved dorsal

skin with 72.2 nmol of 6-CH_3BP-7,8-dihydrodiol in 18 μl of acetone to keep the concentration the same as with the 6-CH_3BP-treated mouse. The mice were killed after 4 h, and the treated areas were excised. The entire 6-CH_3BP-7,8-dihydrodiol-treated skin and half of the 6-CH_3BP-treated skin were incubated with 3 ml of a solution containing proteinase K (60 mg), 2% sodium dodecyl sulfate (1.5 ml), 0.5 M EDTA (3 mL), and H_2O (25.5 ml). The mouse skins were then homogenized in 3 ml Dounce buffer and 30 μl RNAse A. The homogenized skins were placed in Eppendorf tubes and allowed to digest for 3 h or until skin was digested. To isolate the DNA, the digested skins were extracted twice with phenol and three times with $CHCl_3$. The DNA was precipitated with two volumes of absolute C_2H_5OH. The DNA was then removed with a pipette and dissolved in a minimal amount of 0.1 × standard saline citrate buffer to analyze the stable adducts by the ^{32}P-postlabeling method.

2.13. Analysis of depurinating adducts by HPLC and FLNS

The supernatant from each binding reaction (in vitro) or the extract of the epidermis (mouse skin), containing depurinating adducts and metabolites, was evaporated to dryness under vacuum, and the residue was dissolved in DMSO/C_2H_5OH (1:1). After sonication to enhance solubilization, the undissolved residue was removed by centrifugation. The depurinating adducts were analyzed by HPLC, utilizing a Waters 474 scanning fluorescence detector. The depurinating adducts were definitively identified by FLNS after they were separated on HPLC in two different solvent systems (Table 1). The adducts eluting in the second solvent system at the respective retention times of the authentic adducts were collected for identification by FLNS. For each peak, three fractions were collected (early, middle, and late), to assure by FLNS that the peak was homogeneous.

For FLNS identification of collected HPLC fractions, the samples were dried in a speed vac and redissolved in 20 μl of C_2H_5OH with the help of sonication and transferred to quartz tubes (2 mm i.d.), sealed with a rubber septum and cooled by liquid helium in a glass cryostat with quartz optical windows. FLNS was then performed as described above. Detailed discussions on the use of FLNS for fingerprint identification of carcinogen-DNA adducts have been presented by Jankowiak and Small [18,21].

2.14. Calculation of adduct levels

The depurinating adducts were quantitated by comparing the fluorescence peak areas of the adducts biologically-formed to a calibration curve generated from peak areas of known amounts of each of the authentic standards in their respective second solvent system (Table 1). The total amount of each of the adducts was calculated from the calibration curve and normalized to the amount of DNA used in the reaction. The amount of total stable adducts determined by ^{32}P-postlabeling was calculated as previously described [16].

3. Results and discussion

3.1. Synthesis and structure determination of adducts formed by iodine oxidation of 6-CH_3BP in the presence of deoxyribonucleosides or nucleobases

Some adducts were previously synthesized by electrochemical oxidation of 6-CH_3BP in the presence of dAdo or dGuo [7]. The adducts previously identified as BP-6-CH_2-N3Ade and BP-6-CH_2-C8dGuo [7] are, in fact, BP-6-CH_2-N7Ade and BP-6-CH_2-N^2dGuo, respectively. These errors were rectified by the use of 500 MHz NMR [15,22].

One-electron oxidation of 6-CH_3BP produces a radical cation with charge mainly localized at the C-6 position adjacent to the methyl group. Loss of the acidic methyl proton generates a benzylic radical intermediate that is rapidly oxidized to its benzylic carbenium ion (Scheme 1) [12,22]. This intermediate reacts with nucleophilic groups of dGuo, Gua, dAdo, or Ade to form deoxyribonucleoside and/or nucleobase adducts. Iodine oxidation of 6-CH_3BP in the presence of dGuo (Scheme 1) yields the two adducts formed at the 6-CH_3 group, BP-6-CH_2-N7Gua and BP-6-CH_2-N^2dGuo. In addition, adducts are formed competitively at C-1 and C-3, the positions of second highest charge density in the 6-CH_3BP radical cation [7,12], namely, 6-CH_3BP-(1&3)-N7Gua.

Iodine oxidation of 6-CH_3BP in the presence of dGuo, Gua, dAdo or Ade produces an array of adducts that can be used as reference standards in the study of biologically-formed 6-CH_3BP-DNA adducts. The product yields in DMF and DMSO are reported in Table 2. Reaction of the oxidized 6-CH_3BP with dGuo

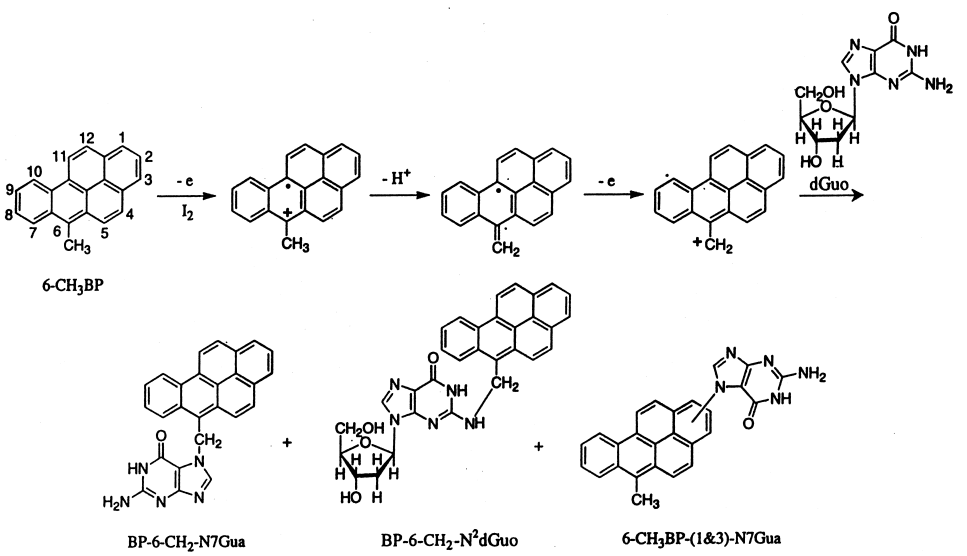

Scheme 1. Proposed mechanism of adduct formation by oxidation of 6-CH_3BP with I_2 in the presence of dGuo.

produced both nucleoside and nucleobase adducts. The use of Gua in the reaction yielded adducts at the same nucleophilic groups as in the reaction with dGuo. More adducts were formed, however, with Ade than with dAdo (Table 2). As observed with BP [6,15], dibenzo[*a*,*l*]pyrene [15,23,24], and other PAH [22,25,26], the deoxyribose moiety of dAdo, bonded at the N-9 of the Ade moiety, prevents reaction of the 6-CH_3BP benzylic carbenium ion at the N-3 position. Therefore, the standard N3Ade adducts of various PAH must be synthesized by reacting the PAH radical cation with Ade.

As noted above, reactions conducted with Ade were analyzed in a C_2H_5OH/CH_3CN/H_2O HPLC solvent system due to the poor resolution of the BP-6-CH_2-N1Ade and 6-CH_3BP-(1&3)-N1Ade adducts in either the CH_3CN/H_2O or CH_3OH/H_2O solvent system (Table 1). The BP-6-CH_2-N1Ade and 6-CH_3BP-(1&3)-N1Ade adducts elute as broad peaks and make it impossible to quantitate accurately each adduct. Therefore, the 6-CH_3BP adducts obtained with Ade were quantitated together and are listed in Table 2 in order of their relative abundance to each other: BP-6-CH_2-N1Ade (most abundant) > 6-CH_3BP-(1&3)-N1Ade > > BP-6-CH_2-N7Ade > BP-6-CH_2-N3Ade (least abundant).

3.1.1. BP-6-CH_2-N7Gua

This compound has UV absorption maxima at 360, 378, and 398 nm, which are typical of 6-substituted BP. FAB MS/MS shows an $(M+H)^+$ ion at m/z 438 for BP-6-CH_2-Gua. In the NMR spectrum of this compound (Fig. 1A), the 6-CH_2 group resonates at 6.25 ppm. NOE irradiation of this chemical shift enhances the signals for 5-H and 7-H at 8.67 and 8.70 ppm, respectively, and the 8-H of Gua at 6.99 ppm. The presence of two 2-NH_2 signals at 6.79 ppm indicates that no substitution has occurred at the 2-NH_2 group. Thus, the Gua moiety must be substituted at the N-7 position.

BP-6-CH_2-N7Gua was not previously identified due to some of its unique chemical properties [7]. This adduct was much more difficult to solubilize in DMSO/CH_3OH (1:1) than any of the other synthesized PAH adducts prior to HPLC analysis. This adduct also exhibited a 'sticky' characteristic that caused it to adhere readily to all unsilated glassware. Two steps were taken to ensure solubilization for both preparative and analytical HPLC. First, all glassware was silated, including reaction flasks and glass vials used to collect the adduct from HPLC. A DMSO/C_2H_5OH (1:1) mixture was also used to dissolve all chemically synthesized or biologically formed BP-6-CH_2-N7Gua. DMSO was needed for solubilization of this adduct to accomplish FAB MS/MS, as well as FLNS.

3.1.2. BP-6-CH_2-N^2dGuo

FAB MS/MS has an $(M+H)^+$ ion at m/z 532 for BP-6-CH_2-dGuo and a fragment at m/z 265, resulting from the loss of dGuo. The proton NMR spectrum (Fig. 1B) shows that the deoxyribose ring is still linked to the Gua base. Protons 1′-H, 2′-H, 3′-H, 4′-H, 5′-H_2, 3′-OH, and 5′-OH are assigned by COSY and by comparison with the spectrum of dGuo. NOE irradiation of the 6-CH_2 group signal at 6.49 ppm shows enhancement of the chemical shifts corresponding to 5-H and

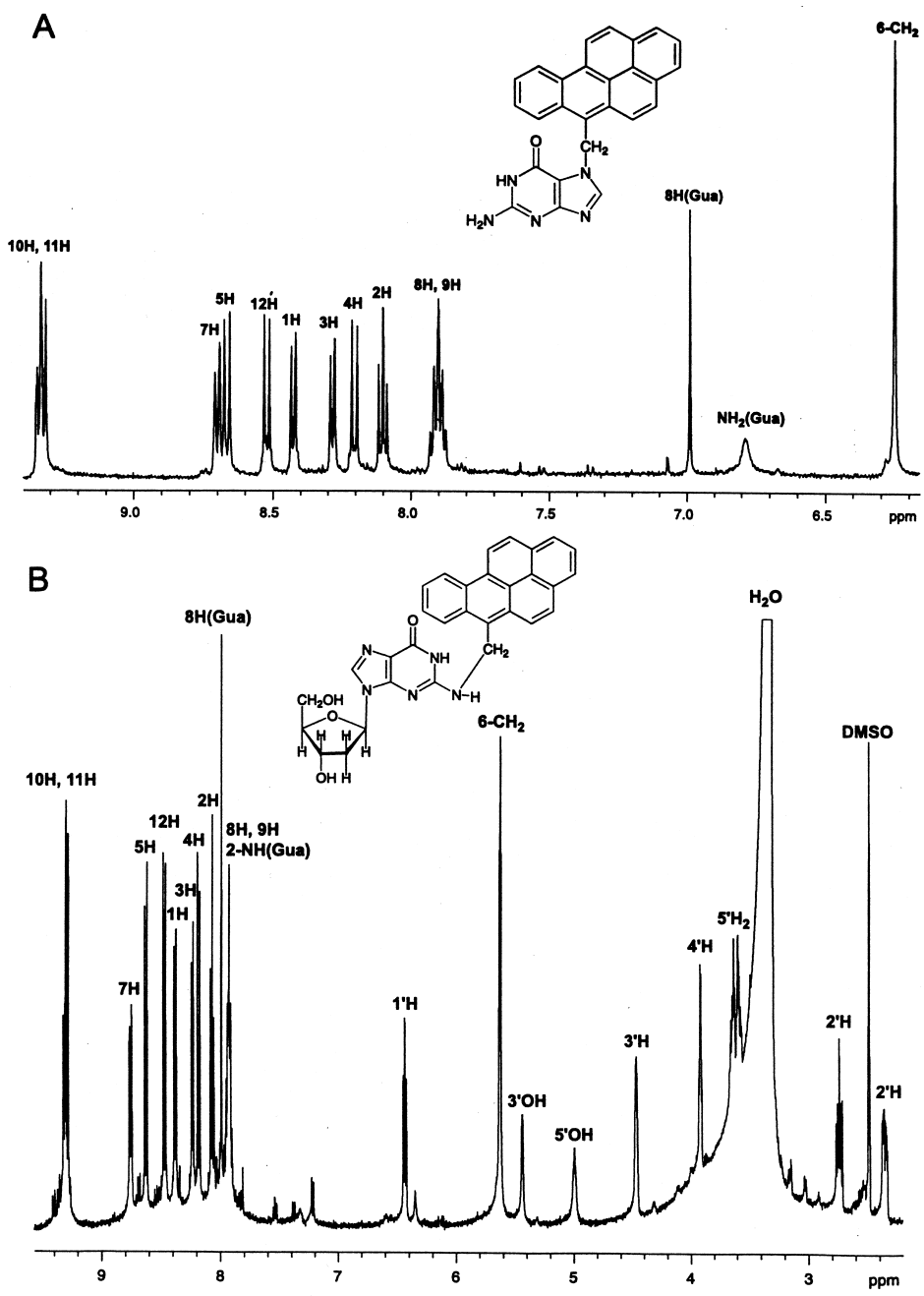

Fig. 1. ^{1}H-NMR spectra of (A) BP-6-CH_2-N7Gua and (B) BP-6-CH_2-N^2dGuo.

7-H at 8.63 and 8.76 ppm, respectively. The D_2O-exchangeable proton with resonance at 7.92 ppm corresponds to the 2-NH group.

3.1.3. BP-6-CH_2-N1Ade

FAB MS/MS exhibits an $(M+H)^+$ ion at m/z 400 for BP-6-CH_2-Ade and a fragment at m/z 265, resulting from the loss of Ade. In the NMR spectrum (Fig. 2A), NOE irradiation of the 6-CH_2 group resonance at 6.72 ppm shows enhancement of the signals for 5-H and 7-H at 8.67 ppm and the 2-H of Ade at 7.64 ppm. This spectrum displays splitting of the two D_2O-exchangeable broad singlet resonances of the NH_2 group at 7.83 and 7.91 ppm. This is characteristic of substitution at the N-1 position (*22*) and is attributed to the close proximity of the aromatic moiety to the 6-amino group that creates a different chemical environment for each of the two protons. The signal for 2-H of Ade is shifted upfield in this molecule, as seen in *meso*-CH_2-N1Ade-linked adducts of 1,2,3,4-tetrahydro-7,12-dimethylbenz[*a*]anthracene [22].

3.1.4. 6-CH_3BP-(1&3)-N1Ade

FAB MS shows the $(M+H)^+$ ion at m/z 400 for 6-CH_3BP-Ade. The NMR spectrum (Fig. 2B) reveals the presence of a mixture of two isomers in which Ade is linked to C-1 or C-3 of the 6-CH_3BP moiety in a ratio of 75:25, respectively. The two isomers, 6-CH_3BP-1-N1Ade and 6-CH_3BP-3-N1Ade, were not separated due to their almost identical physico-chemical properties. One of the characteristics of the NMR spectrum is the shift upfield of the 4-H resonance of the C-3 isomer and the 12-H resonance of the C-1 isomer, as determined by COSY. The same shift upfield occurs for the 8-H[Ade] that is characteristic of the N1Ade adducts with the bond at the C-6 of BP [6]. Furthermore, NOE irradiation of the 6-CH_3 group at 3.22 ppm shows enhancement of the signals for 5-H(3) at 8.38 ppm and 5-H(1) and 7-H(1,3) at 8.65 ppm. The splitting of the two D_2O-exchangeable broad singlet signals of the NH_2 group at 8.25 and 8.33 ppm is similar to that of the other N1Ade adducts [6,22].

3.1.5. BP-6-CH_2-N3Ade

FAB MS/MS shows an $(M+H)^+$ ion at m/z 400 for BP-6-CH_2-Ade and a fragment at m/z 265, resulting from the loss of Ade. NOE irradiation of the 6-CH_2 group resonance at 6.49 ppm in the NMR spectrum (Fig. 3A) of this adduct shows enhancement of the signals for 5-H and 7-H at 8.74 ppm, and the 2-H of Ade at 7.56 ppm, similarly to those seen in BP-6-CH_2-N1Ade. The D_2O-exchangeable broad singlet signal of the NH_2 group is observed at 7.28 ppm of the NMR spectrum. This adduct is not formed by iodine oxidation of 6-CH_3BP in the presence of dA, as discussed above.

3.1.6. BP-6-CH_2-N7Ade

FAB MS/MS exhibits an $(M+H)^+$ ion at m/z 400 for BP-6-CH_2-Ade. In the NMR spectrum (Fig. 3B), NOE irradiation of the 6-CH_2 group resonance at 6.72 ppm shows enhancement of the signals for 5-H and 7-H at 8.46 ppm, and the 8-H

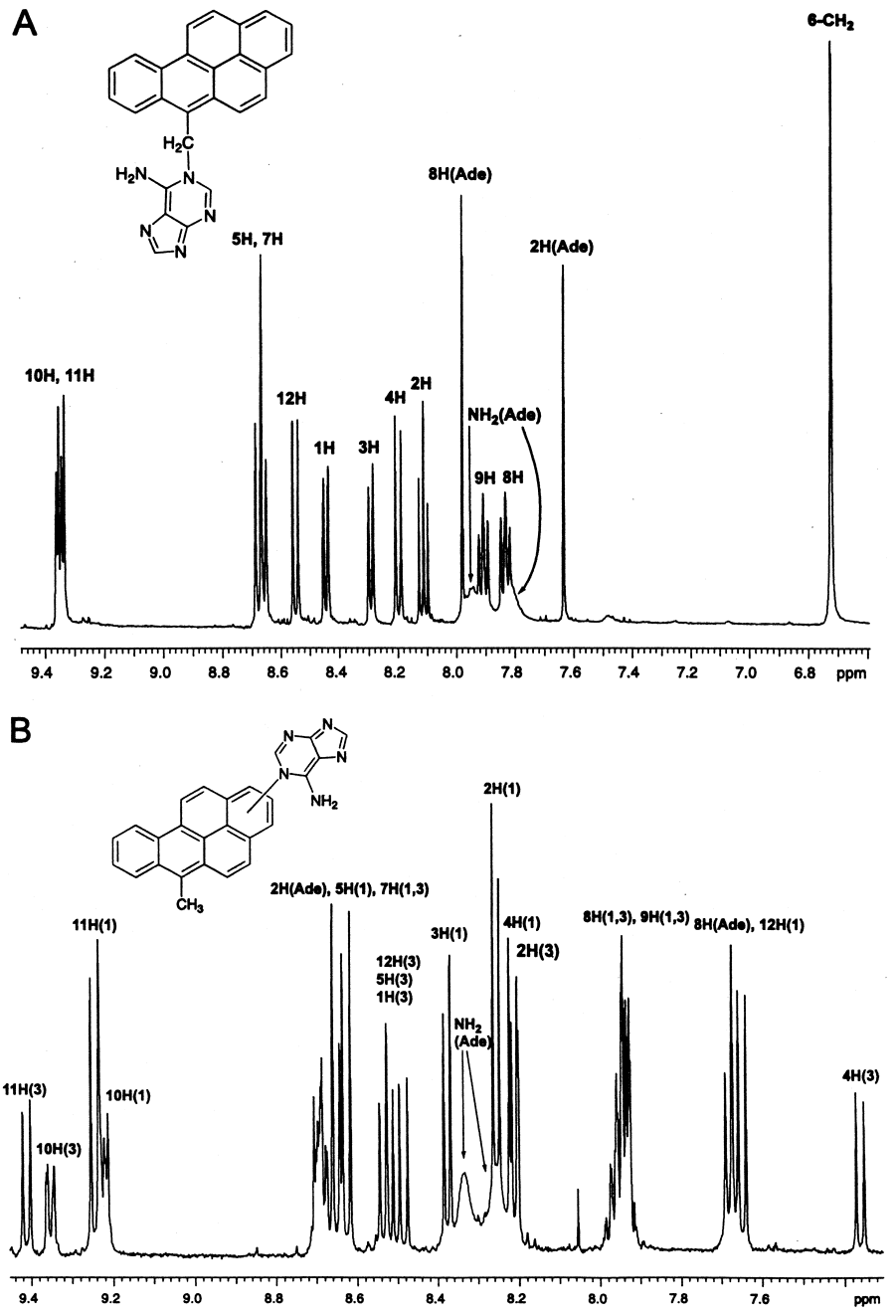

Fig. 2. ^{1}H-NMR spectra of (A) BP-6-CH_2-N1Ade and (B) 6-CH_3BP-(1&3)-N1Ade.

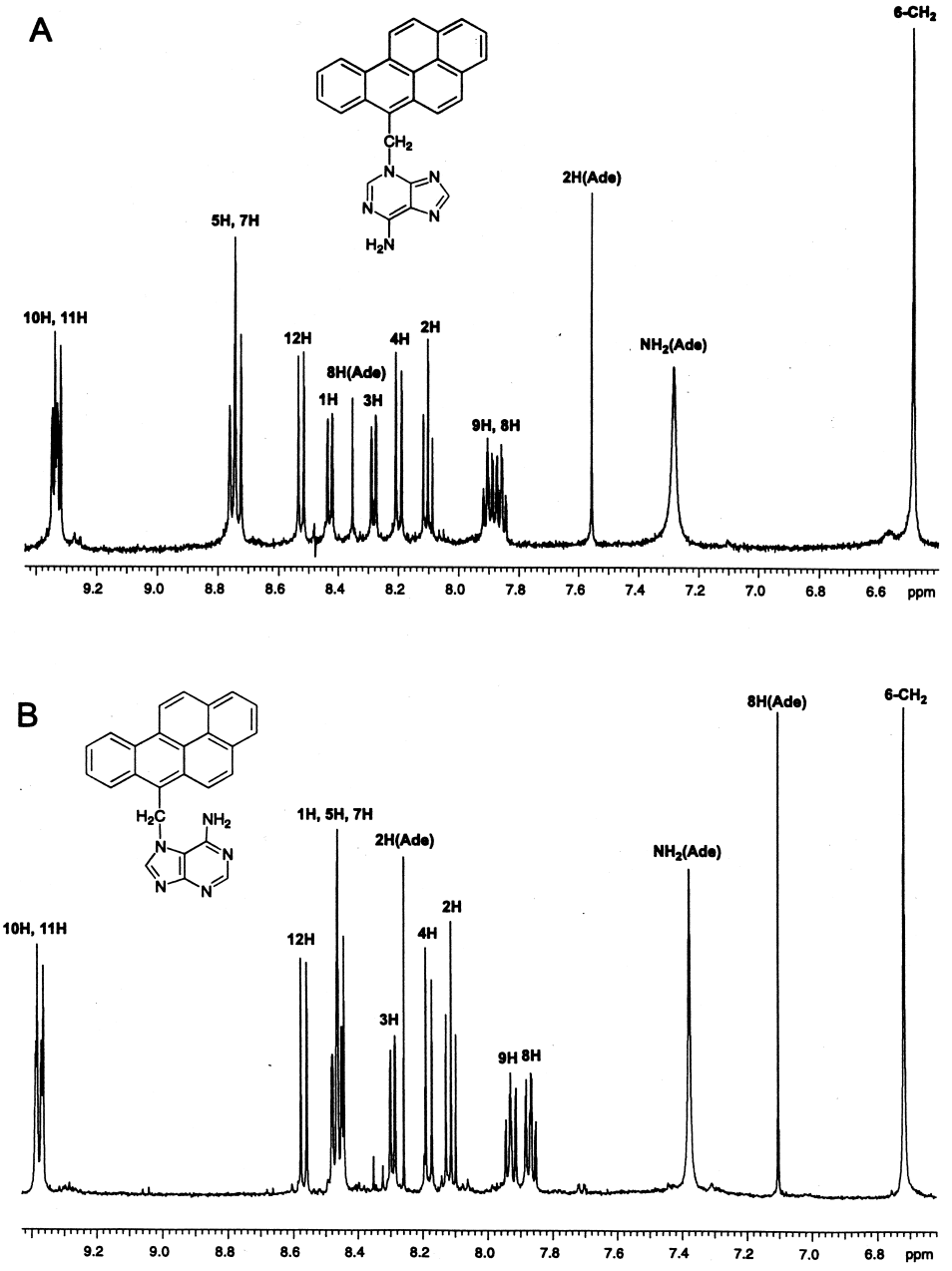

Fig. 3. ^{1}H-NMR spectra of (A) BP-6-CH_2-N3Ade and (B) BP-6-CH_2-N7Ade.

of Ade at 7.10 ppm. The D_2O-exchangeable broad singlet signal of the NH_2 group is observed at 7.38 ppm of the NMR spectrum.

3.1.7. BP-6-CH_2-N3dThd

For the first time, electrochemical oxidation of a PAH yielded an adduct with dThd. FAB MS/MS shows an $(M+H)^+$ ion at m/z 507 for the BP-6-CH_2-dThd adduct and a fragment of 243, resulting from the loss of the BP-6-CH_2 group. The NMR spectrum of this compound (Fig. 4) clearly indicates that this is a 6-CH_3BP-dThd stable adduct due to the presence of both 6-CH_3BP and dThd proton signals. The chemical shifts of the dThd moiety resemble those of dThd, supporting that the only logical portion linked to the BP-6-CH_2 moiety is the N-3 of the dThd. The downfield shift of the 6-CH_2 proton resonance indicates that this group is bound to an electron-withdrawing atom such as N. Furthermore, the multiplet signal of the CH_2 protons, coupling to each other, confirms the bond of CH_2 to the chiral nitrogen group.

3.2. Identification of DNA adducts in vitro and in mouse skin

The 6-CH_3BP adducts formed by cytochrome P450 activation in MC-induced rat liver microsomes in the presence of calf thymus DNA or in 6-CH_3BP-treated mouse skin were compared to those formed by HRP, a model for formation of adducts by one-electron oxidation. The total stable adducts formed were quantitated by the ^{32}P-postlabeling method [16]. The depurinating adducts were identified by comparison of their HPLC elution times and their FLN spectra with those of synthesized adduct standards. Quantitation of the depurinating adducts, whenever possible, was accomplished by HPLC with fluorescence detection as described above.

3.3. Depurinating adducts

The appropriate retention times for the depurinating adducts were first established by injecting a small amount of adduct standards. This was followed by analysis of the biologically formed adducts. Analytes of interest were separated by HPLC in two consecutive solvent systems, starting wih a CH_3CN/H_2O gradient (Table 1). Fractions from this separation were collected at retention times corresponding to the appropriate guanine and/or adenine standard adducts. The analyte corresponding to the retention time of the 6-CH_3BP-(1&3)-N7Gua adduct standard was then rechromatographed with a CH_3OH/H_2O gradient. Since BP-6-CH_2OH elutes at the same time as BP-6-CH_2-N7Gua in both CH_3CN/H_2O and CH_3OH/H_2O gradients, a third solvent system ($C_2H_5OH/CH_3CN/H_2O$, Table 1) was utilized to purify the BP-6-CH_2-N7Gua adduct for fluorescence and quantitation studies. HPLC data (chromatograms not shown) suggested that 6-CH_3BP, in the presence of DNA, is activated by both cytochrome P450 and HRP to form two depurinating adducts by the radical cation pathway, BP-6-CH_2-N7Gua and 6-CH_3BP-(1&3)-N7Gua (Table 3). The same depurinating adducts seemed to be formed in 6-CH_3BP-treated mouse skin. Definite proof of the structures was obtained by FLNS analysis as shown below.

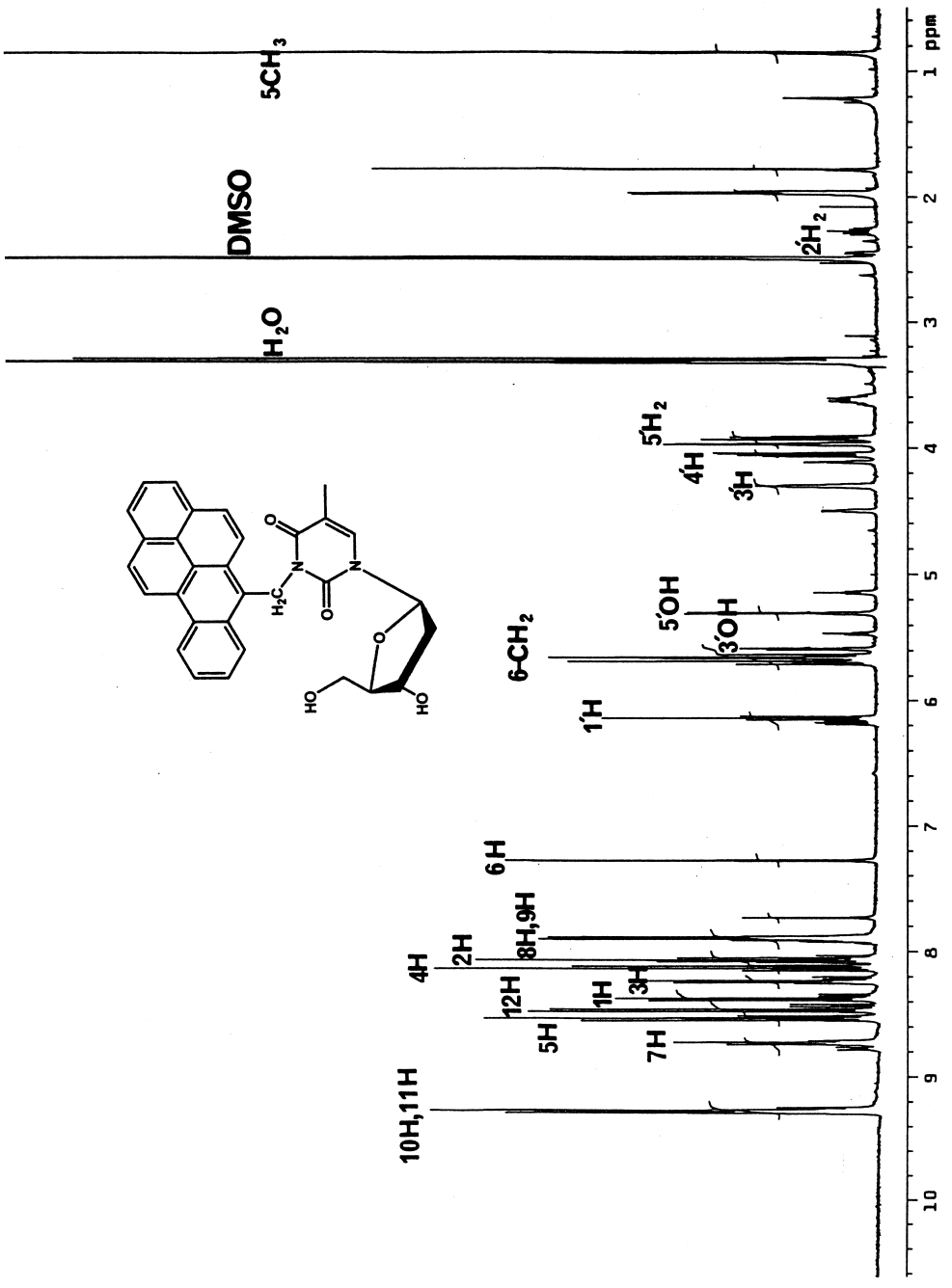

Fig. 4. ^{1}H-NMR spectrum of BP-6-CH_2-N3dThd.

Table 3
Quantitation of biologically-formed 6-CH_3BP-DNA adducts

Biological system	Total adducts, μmol/mol of DNA-P	Total stable DNA adducts, μmol/mol of DNA-P[a]	Depurinating DNA adducts, μmol/mol of DNA-P			Ratio of depurinating/stable adducts
			BP-6-CH_2-N7Gua	6-CH_3BP-(1&3)N7Gua	Total depurinating adducts	
HRP	3.25	0.93[b] (29)[c]	1.57[d] (48)	0.75[d] (23)	2.32 (71)	2.46
Microsomes	7.01	4.74[e] (68)	1.55[b] (22)	0.72[b] (10)	2.27 (32)	0.47
Mouse skin		0.020[d]	+[f]	+[f]		

[a] These adducts have not been identified.
[b] Values are an average from three preparations.; replicate values differed by ≤20%
[c] Number in parentheses is percentage of total adducts.
[d] Values are an average from two preparations.; replicate values differed by ≤20%
[e] Values are an average from six preparations.; replicate values differed by ≤20%
[f] The adducts were identified by FLNS, but interference of metabolites makes quantitation impossible.

3.3.1. Non-line narrowed (NLN) spectra

For the BP-6-CH_2-N7Gua adduct, the 77 K fluorescence spectrum obtained under NLN conditions revealed a single (0,0)-fluorescence band at 407.0 nm. In contrast, the NLN spectrum obtained for the 6-CH_3BP-(1&3)-N7Gua standard revealed two origin bands at 409 and 414 nm, which tentatively can be attributed to the two isomers, as demonstrated by NMR spectroscopy [7]. To identify the bands corresponding to the C-1 and C-3 isomers, the above data were compared to results obtained for BP substituted with a methoxy group at C-1 and C-3, which have origin bands at $\sim$414 and $\sim$423 nm [27]. This comparison suggests that the two components of the 6-CH_3BP-(1&3)-N7Gua adduct, observed at 409 and 414 nm, most probably correspond to the 6-CH_3BP-1-N7Gua and 6-CH_3BP-3-N7Gua isomers, respectively. Similar ratios of the two isomers, not separable by HPLC, were observed in vitro and in mouse skin. Because the fluorescence quantum yield of these two isomers is not known, their relative contribution could not, however, be assessed by fluorescence studies.

3.3.2. BP-6-CH_2-N7Gua

The BP-6-CH_2-N7Gua adduct was identified by FLNS (Fig. 5). Frames A and B, obtained at 4.2 K with excitation wavelength of 386.0 and 397.0 nm, respectively, reveal different regions of the vibronic spectrum. The top spectra are those of the

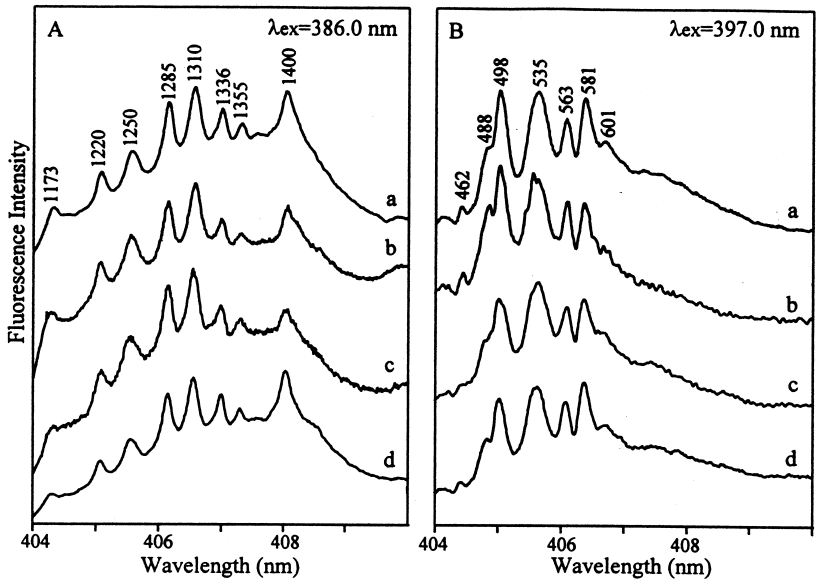

Fig. 5. Comparison of the vibronically excited FLN spectra of the BP-6-CH_2-N7Gua adduct standard (curves a) with FLN spectra of HPLC fractions from HRP-catalyzed reaction (curves b), microsome-catalyzed reaction (curves c), and from mouse skin (curves d). Frames A and B were obtained for $\lambda_{ex} = 386.0$ and 397.0 nm, respectively; $T = 4.2$ K. The FLN peaks are labeled with their excited-state vibrational frequencies in cm^{-1}.

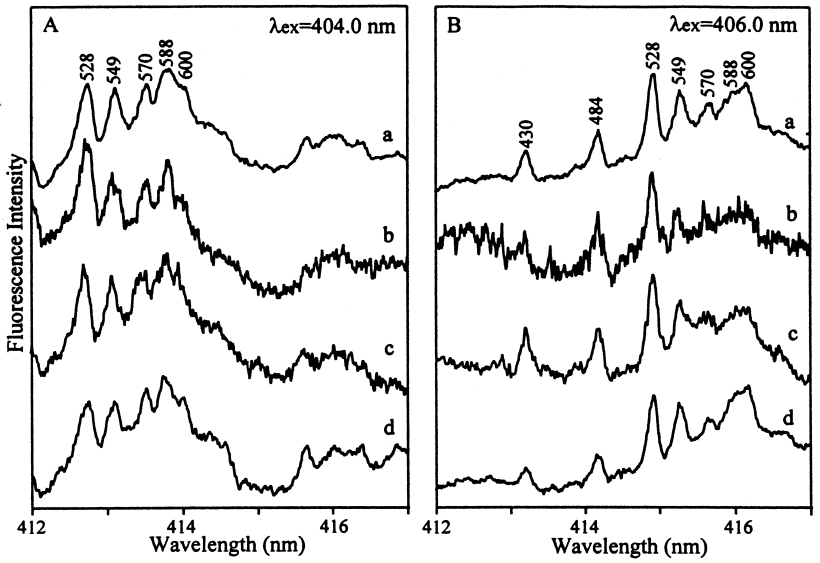

Fig. 6. FLNS identification of the 6-CH_3BP-(1&3)-N7Gua adduct. Frames A and B were obtained for excitation wavelength of 404.0 and 406.0 nm, respectively. Spectra a correspond to the adduct standard, whereas spectra b, c and d are the FLN spectra corresponding to the HPLC fraction obtained with HRP, microsomes, and mouse skin, respectively. The FLN peaks are labeled with their excited-state vibrational frequencies in cm^{-1}. $T = 4.2$ K.

authentic adduct standard. The numbers, e.g. 1173, 1220, 1250, etc., label the excited vibrational frequencies in cm^{-1}. Comparison of the standard spectra (curves a) with those obtained for the corresponding adduct formed with HRP (b), with microsomes (c), and in mouse skin (d), illustrates the identification power of FLNS. The spectra are indistinguishable, proving that the HPLC fractions from the HRP- and microsome-catalyzed reactions and from mouse skin eluting at the retention time of the BP-6-CH_2-N7Gua adduct standard indeed contained that compound. Matching spectra were also obtained for several other excitation wavelengths (spectra not shown). Finally, the characteristic modes of the BP-6-CH_2-N7Gua adduct were completely different from those observed for the major metabolite, BP-6-CH_2OH. For example, the typical low-frequency modes observed for the metabolite (data not shown) were 454, 475, 508, 546, and 567 cm^{-1}, in contrast to 462, 488, 498, 535, and 563 cm^{-1} observed for the BP-6-CH_2-N7Gua adduct.

3.3.3. 6-CH_3BP-(1&3)-N7Gua

The standard FLN spectra of the 6-CH_3BP-(1&3)-N7Gua adduct are shown as the upper spectra (a) in Fig. 6. Excitation wavelengths of 404.0 (frame A) and 406.0 nm (frame B) provide the S_1 state vibronic excitations of the 6-CH_3BP chromophore, and prominent zero-phonon origin lines due to $\sim$400-600 cm^{-1} vibrations are observed. Spectra b, c and d correspond to the depurinating adducts

isolated from HRP and microsome preparations, and from mouse skin, respectively. Only portions of the FLN spectra in the region of ~414 are shown in Fig. 6. These spectra are identical to those of the synthesized standard; identical spectra were also observed in the 408-nm region (not shown). Thus, the second major isolated depurinating adduct is 6-CH_3BP-(1&3)-N7Gua.

3.3.4. BP-6-CH_2-Ade adducts

HPLC peaks corresponding to the synthesized authentic standard of BP-6-CH_2-N3Ade and BP-6-CH_2-N7Ade were also collected and rechromatographed in two different solvent systems (Table 1). No peak corresponding to the retention time of BP-6-CH_2-N3Ade was detected in any of the *in vitro* or mouse skin experiments. Although in the second solvent system (Table 1) a peak matching the retention time of the standard of BP-6-CH_2-N7Ade was collected, its identity was not confirmed by FLNS. Thus, all of the depurinating adducts identified were formed at guanine residues.

3.4. Stable adducts

The profiles of adducts observed by ^{32}P-postlabeling after activation of 6-CH_3BP by HRP (Fig. 7A) and microsomes (Fig. 7B) contained many similarities in the less-polar region, although a number of more polar adducts were seen with HRP. These profiles closely resemble ones previously obtained (Fig. 4 in [8]), although some of the more polar adducts were cut off the previous profile for HRP (Fig. 4B in [8]). The profile of adducts observed in mouse skin (Fig. 7C) also has similarities with the adducts observed after activation by HRP or microsomes, although the level of adducts is much lower (Table 3). To establish whether 6-CH_3BP forms diol epoxide adducts in mouse skin, 6-CH_3BP-7,8-dihydrodiol was prepared by microsomal metabolism, which gave a very poor yield. An experiment comparing the stable adducts formed in the skin of a 6-CH_3BP- or 6-CH_3BP-7,8-dihydrodiol-treated mouse was performed, and the profile of adducts observed with the dihydrodiol (Fig. 7D) suggests that the 7,8-dihydrodiol-9,10-epoxide contributes somewhat to the stable 6-CH_3BP adducts. These results show that 6-CH_3BP-7,8-dihydrodiol can be metabolized to its presumed diol epoxide and react with DNA, in contrast to the results (published in ref. [8]), in which microsomes did not form DNA adducts from 6-CH_3BP-7,8-dihydrodiol (Fig. 4B in [8]). This indicates that the pseudodiaxial 6-CH_3BP-7,8-dihydrodiol forms the 7,8-diol-9,10-epoxide similarly to the pseudodiequatorial BP-7,8-dihydrodiol. In fact, this was previously observed for conversion of the pseudodiaxial 6-fluoroBP-7,8-dihydrodiol to its diol epoxide [8,28].

3.5. Quantitation of DNA adducts

Quantitation of total stable adducts was accomplished by the ^{32}P-postlabeling method (Table 3), but the amounts of the individual adducts were not compared. Quantitation of depurinating adducts was achieved by HPLC with fluorescence detection. Microsomal and HRP activation of 6-CH_3BP in the presence of DNA

produced similar amounts of the two depurinating guanine adducts (Table 3). Microsomal preparations produced 32% depurinating adducts, whereas HRP activation yielded 71%. Microsomal activation afforded five times more stable adducts than HRP. The depurinating adducts that might be formed from 6-CH_3BP-7,8-diol-9,10-epoxide were not synthesized. The very low level of depurinating adducts formed by BP-7,8-diol-9,10-epoxide in mouse skin (5% of the stable adducts) [6] and the poor conversion of 6-CH_3BP to its 7,8-dihydrodiol (at least ten times lower than that with BP) suggest that the depurinating adducts by this pathway are formed at best in trace amounts.

Due to interference by 6-CH_3BP metabolites during HPLC purification, the depurinating adducts formed in 6-CH_3BP-treated mouse skin could not be quantitated. 6-CH_3BP-treated mouse skin contained 200-fold lower levels of stable adducts than observed with microsome-activated 6-CH_3BP and 50 times less than with HRP-activated 6-CH_3BP (Table 3).

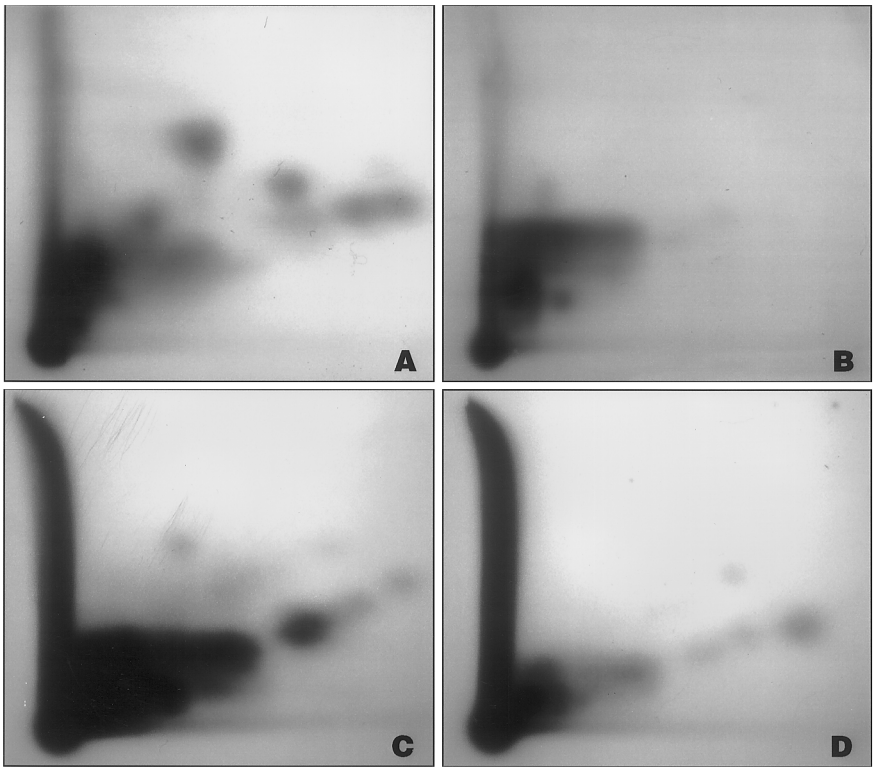

Fig. 7. Autorqadiograms of ^{32}P-postlabeled DNA containing adducts formed after (A) activation of 6-CH_3BP by HRP, (B) activation 0f 6-CH_3BP by microsomes, (C) reaction of 6-CH_3BP with mouse skin and (D) reaction of 6-CH_3BP-7,8-dihydrodiol with mouse skin. The film was exposed for (A) 3 h at room temperature, (B) 3 h at room temperature, (C) 24 h at -80°C, or (D) 24h at -80°C.

Although BP-6-CH_2-N7Gua and 6-CH_3BP-(1&3)-N7Gua could not be quantitated, approximately 0.11 μmol/mol DNA is the limit of detection for positive FLNS identification of these two 6-CH_3BP-N7Gua adducts. Therefore, assuming that at least 0.11 μmol/mol DNA of each of the 6-CH_3BP-N7Gua depurinating adducts is present in mouse skin and the stable adducts are present at 0.020 μmol/mol DNA (Table 3), these two depurinating adducts are the predominant adducts formed in mouse skin.

4. Conclusions

Reaction of the 6-CH_3BP radical cation in chemical and biological systems occurs competitively at the 6-CH_3 group and at C-1 and C-3, the positions of second highest charge density in its radical cation. Depurinating adducts of 6-CH_3BP are formed in vitro and in mouse skin only at guanine bases. Furthermore, for the first time, a PAH radical cation was found to produce an adduct with thymidine, the stable adduct BP-6-CH_2-N3dThd.

6-CH_3BP is much less carcinogenic than BP [9,11]. In biological systems, 6-CH_3BP produces depurinating DNA adducts through the one-electron oxidation pathway. Depurinating DNA adducts have been correlated with Harvey-*ras* mutations in mouse skin papillomas and have been suggested to be the primary culprit generating mutations leading to cancer [3,4]. Thus, the weaker tumor-initiating activity of 6-CH_3BP compared to that of BP [11] could be the consequence of the weaker reactivity of 6-CH_3BP radical cation compared to that of BP radical cation.

Acknowledgements

We gratefully thank Dr. Ronald Cerny at the Nebraska Center for Mass Spectrometry at the University of Nebraska-Lincoln for the valuable mass spectral data. We extend our deepest gratitude to Paula Mailander and Dr. Dhruba Chakravarti for help in isolating DNA from 6-CH_3BP-7,8-dihydrodiol-treated mouse skin. We would also like to thank Sheila Higginbotham for her help with the mouse skin experiments. This research was supported by a US PHS grant from the National Cancer Institute (P01 CA49210). Core support at the Eppley Institute was funded by NCI Laboratory Cancer Research Center Support (Core) Grant CA36727. Aaron Hanson received fellowship support from the Eppley Institute, the University of Nebraska Center for Environmental Toxicology and the University of Nebraska Medical Center.

References

[1] E.L. Cavalieri, E.G. Rogan, The approach to understanding aromatic hydrocarbon carcinogenesis. The central role of radical cations in metabolic activation, Pharmacol. Ther. 55 (1992) 183–199.

[2] E.L. Cavalieri, E.G. Rogan, Mechanisms of tumor initiation by polycyclic aromatic hydrocarbons in mammals, in: A.H. Neilson (Ed.), The Handbook of Environmental Chemistry: PAHs and Related Compounds, vol. 3J, Springer, Heidelberg, 1998, pp. 81–117.
[3] M. Hall, P.L. Grover, Polycyclic aromatic hydrocarbons: metabolisms, activation and tumor initiation, in: C.S. Cooper, P.L. Grover (Eds.), Chemical Carcinogenesis and Mutagenesis, Springer, Heidelberg, 1990, pp. 327–372.
[4] D. Chakravarti, J.C. Pelling, E.L. Cavalieri, E.G. Rogan, Relating aromatic hydrocarbon-induced DNA adducts and c-Harvey-*ras* mutations in mouse skin papillomas: The role of apurinic sites, Proc. Natl. Acad. Sci. USA 92 (1995) 10422–10426.
[5] E.G. Rogan, P.D. Devanesan, N.V.S. RamaKrishna, S. Higginbotham, N.S. Padmavathi, K. Chapman, E.L. Cavalieri, H. Jeong, R. Jankowiak, G.J. Small, Identification and quantitation of benzo[*a*]pyrene-DNA adducts formed in mouse skin, Chem. Res. Toxicol. 6 (1993) 356–363.
[6] L. Chen, P.D. Devanesan, S. Higginbotham, F. Ariese, R. Jankowiak, G.J. Small, E.G. Rogan, E.L. Cavalieri, Expanded analysis of benzo[*a*]pyrene-DNA adducts formed in vitro and in mouse skin: their significance in tumor initiation, Chem. Res. Tox. 9 (1996) 897–903.
[7] N.V.S. RamaKrishna, K.-M. Li, E.G. Rogan, E.L. Cavalieri, M. George, R.L. Cerny, M.L. Gross, Adducts of 6-methylbenzo[*a*]pyrene and 6-fluorobenzo[*a*]pyrene formed by electrochemical oxidation in the presence of deoxyribonucleosides, Chem. Res. Toxicol. 6 (1993) 837–845.
[8] R. Todorovic, P.D. Devanesan, E.G. Rogan, E.L. Cavalieri, ^{32}P-postlabeling analysis of the DNA adducts of 6-fluorobenzo[*a*]pyrene and 6-methylbenzo[*a*]pyrene formed in vitro, Chem. Res. Toxicol. 6 (1993) 530–534.
[9] E. Cavalieri, R. Roth, C. Grandjean, J. Althoff, K. Patil, S. Liakus, S. Marsh, Carcinogenicity and metabolic profiles of 6-substituted benzo[*a*]pyrene derivatives on mouse skin, Chem. Biol. Interact. 22 (1978) 53–68.
[10] E. Cavalieri, E. Rogan, S. Higginbotham, P. Cremonesi, S. Salmasi, Tumorigenicity of 6-halogenated derivatives of benzo[*a*]pyrene in mouse skin and rat mammary gland, J. Cancer Res. Clin. Oncol. 114 (1988) 10–15.
[11] E. Cavalieri, E. Rogan, S. Higginbotham, P. Cremonesi, S. Salmasi, Tumor initiating activity in mouse skin and carcinogenicity in rat mammary gland of fluorinated derivatives of benzo[*a*]pyrene and 3-methylcholanthrene, J. Cancer Res.Clin. Oncol. 114 (1988) 16–22.
[12] P. Cremonesi, E.L. Cavalieri, E.G. Rogan, One-electron oxidation of 6- substituted benzo[*a*]pyrenes by manganic acetate. A model for metabolic activation, J. Org. Chem. 54 (1989) 3561–3570.
[13] E.G. Rogan, E.L. Cavalieri, S. Tibbels, P. Cremonesi, C. Warner, D. Nagel, K. Tomer, R. Cerny, M. Gross, Synthesis and identification of benzo[*a*]pyrene- guanine nucleoside adducts formed by electrochemical oxidation and horseradish peroxidase-catalyzed reaction of benzo[*a*]pyrene with DNA, J. Am. Chem. Soc. 110 (1988) 4023–4029.
[14] N.V.S. RamaKrishna, F. Gao, N.S. Padmavathi, E.L. Cavalieri, E.G. Rogan, R.L. Cerny, M.L. Gross, Model adducts of benzo[*a*]pyrene and nucleosides formed from its radical cation and diol epoxide, Chem. Res. Toxicol. 5 (1992) 293–302.
[15] A.A. Hanson, E.G. Rogan, E.L. Cavalieri, Synthesis of adducts formed by iodine oxidation of aromatic hydrocarbons in the presence of deoxyribonucleosides and nucleobases, Chem. Res. Toxicol. 11 (1998) 1201–1208.
[16] W.J. Bodell, P.D. Devanesan, E.G. Rogan, E.L. Cavalieri, ^{32}P-postlabeling analysis of benzo[*a*]pyrene-DNA adducts formed in vitro and in vivo, Chem. Res. Toxicol. 2 (1989) 312–315.
[17] *NIH Guidelines for the Laboratory Use of Chemical Carcinogens*; NIH Publication No. 81-2385; Washington, DC: US Government Printing Office, 1981.
[18] R. Jankowiak, G.J. Small, Fluorescence line narrowing: a high-resolution window on DNA and protein damage from chemical carcinogens, Chem. Res. Toxicol. 4 (1991) 256–269.
[19] F. Dewhurst, D.A. Kitchen, Synthesis and properties of 6-substituted benzo[*a*]pyrene derivatives, J. Chem. Soc. Perkin Trans. I (1972) 710–712.
[20] E.L. Cavalieri, E.G. Rogan, P.D. Devanesan, P. Cremonesi, R.L. Cerny, M.L. Gross, W.J. Bodell, Binding of benzo[*a*]pyrene to DNA by cytochrome P-450-catalyzed one-electron oxidation in rat liver microsomes and nuclei, Biochemistry 29 (1990) 4820–4827.

[21] R. Jankowiak, G.J. Small, Fluorescence line-narrowing spectroscopy in the study of chemical carcinogenesis, Anal. Chem. 61 (1989) 1023A–1032A.
[22] P.P.J. Mulder, L. Chen, B.C. Sekhar, M. George, M.L. Gross, E.G. Rogan, E.L. Cavalieri, Synthesis and structure determination of the adducts formed by electrochemical oxidation of 1,2,3,4-tetrahydro-7,12-dimethylbenz[*a*]anthracene, Chem. Res. Toxicol. 9 (1996) 1264–1277.
[23] N.V.S. RamaKrishna, N.S. Padmavathi, E.L. Cavalieri, E.G. Rogan, R.L. Cerny, M.L. Gross, Synthesis and structure determination of the adducts formed by electrochemical oxidation of the potent carcinogen dibenzo[*a*,*l*]pyrene in the presence of nucleosides, Chem. Res. Toxicol. 6 (1993) 554–560.
[24] K.-M. Li, J. Byun, M.L. Gross, D. Zamzow, R. Jankowiak, E.G. Rogan, E.L. Cavalieri, Synthesis and structure determination of the adducts formed by electrochemical oxidation of dibenzo[*a*,*l*]pyrene in the presence of adenine, Chem. Res. Toxicol. 12 (1999) 749–757.
[25] N.V.S. RamaKrishna, E.L. Cavalieri, E.G. Rogan, G. Dolnikowski, R.L. Cerny, M.L. Gross, H. Jeong, R. Jankowiak, G.J. Small, Synthesis and structure determination of the adducts of the potent carcinogen 7,12-dimethylbenz[*a*]anthracene and deoxyribonucleosides formed by electrochemical oxidation: models for metabolic activation by one-electron oxidation, J. Am. Chem. Soc. 114 (1992) 1863–1874.
[26] L. Chen, P.D. Devanesan, J. Byun, J.K. Gooden, M.L. Gross, E.G. Rogan, E.L. Cavalieri, Synthesis of depurinating DNA adducts formed by one-electron oxidation of 7H-dibenzo[*c*,*g*]carbazole and identification of these adducts after activation with rat liver microsomes, Chem. Res. Toxicol. 10 (1997) 225–233.
[27] F. Ariese, S.J. Kok, M. Verkaik, Chemical derivatization and Shpol'skii spectrofluorometric determination of benzo[*a*]pyrene metabolites in fish bile, Anal. Chem. 65 (1993) 1100–1106.
[28] D.R. Buhler, F. Unlu, D.R. Thakker, T.J. Slaga, A.H. Conney, A.W. Wood, R.L. Chang, W. Levin, D.M. Jerina, Effect of a 6-fluoro substituent on the metabolism and biological activity of benzo[*a*]pyrene, Cancer Res. 43 (1983) 1541–1549.